Journal Name

ARTICLE TYPE

Cite this: DOI: 00.0000/xxxxxxxxxx

The Superprotonic Transition is Facilitated by a Decrease in Entropic Restrictions†

Iván Santamaría-Holek,*[a,‡] Aldo Ledesma-Durán,[a] S. I. Hernández-Hernández,[b] C. García-Alcántara,[b] Andreu Andrio,[c] Vicente Compañ[d]

Received Date
Accepted Date

DOI: 00.0000/xxxxxxxxxx

The crystallographic structure of solid electrolytes and other materials determines the protonic conductivity in devices as fuel cells, ionic-conductors and supercapacitors. Experiments show that a rise of the temperature in a narrow interval may lead to a sudden increase of several orders of magnitude of the conductivity of some materials, a process called superprotonic transition. Here, we show that the change of entropic restrictions associated with solid-solid phase or structural transitions controls the superprotonic transition and therefore the ionic conductivity in these systems. A novel macro-transport theory for irregular domains is formulated for this purpose and used to deduce a general formula for the temperature dependence on the ionic conductivity. The formula fits remarkably experimental data of superprotonic transition in doped cesium phosphates and other materials reported in the literature.

1 Introduction

The ion conductance in amorphous solids, crystals, quasi-crystals, polycrystals and their compounds has become a very important field of technological, experimental and theoretical research due to the urgent demand of substituting fossil fuels by more efficient and cleaner energy resources. The challenge is of the major importance and difficulty since the practical operation of micro-, meso- and macroscopic devices involves high energy dissipation during chemo-electrical conversion and, therefore, the raise of large temperature changes during operation and rest. These facts make clear the necessity of a precise understanding of the processes of (super)protonic and, in general, ionic conductivity in fuel cells, batteries and super-capacitors. In this context, transitions between different crystal phases or vitreous states are significant during operation and rest since they can be used as thermally controlled mechanisms for the transition between a storage device (at lower temperatures) and an active fuel cell (at higher temperatures), in such a way that changes in the conductivity of several orders of magnitude are welcome in a temperature range of few Kelvin degrees. This behavior, called superprotonic transition may be used as a control mechanism of the ionic conductivity and it has been examined experimentally for several systems[1–7]. Here, we include recent results of the referred phase transitions between monoclinic and cubic phases of CsP and a mixture based on the partial substitution of Cs by Rb.[8] These phase transitions induce a sudden change of three orders of magnitude of the ion conductance[8]. In what follows we propose a simple and direct macro-transport theory from which we deduce a general formula accounting for the complex *non-isothermal* conductance $G_\nu(T)$ of solid and aqueous fuel cells in the temperature range including the superprotonic transition[9,10].

Dielectric spectroscopy experiments[8] measure the homogeneous frequency (ν) dependent conductance $G_\nu(T)$ at different temperatures (T). In contrast, the mathematical description of charge carriers transport is provided in terms of a generalized Fick's law involving an ion current density $\mathbf{i}(\mathbf{r},t)$ that depends on position $\mathbf{r}$ and time t. With the aim to deduce an homogeneous macro-transport coefficient we will perform the implicit volume average present in experiments along the lines of a recently proposed theoretical description of mass transport across confined spaces.[11,12] The key idea is that the transport along the main (longitudinal) coordinate due to an imposed electrical field is, in general, strongly influenced by the spatial arrangement of the molecules in the material. This arrangement is determined by the crystallographic phase, thus suggesting the presence of

[a] *Centro de Física Aplicada y Tecnología Avanzada CFATA, Universidad Nacional Autónoma de México (UNAM), Juriquilla, Querétaro, CP 76230, Mexico; E-mail: isholek.fc@gmail.com.*

[b] *Unidad Multidisciplinaria de Docencia e Investigación-Juriquilla, Facultad de Ciencias, Universidad Nacional Autónoma de México (UNAM), Juriquilla, Querétaro, CP 76230, Mexico.*

[c] *Departamento de Física, Universitat Jaume I, 12080-Castellón de la Plana, Spain.*

[d] *Departamento de Termodinámica Aplicada, Universitat Politécnica de Valencia, C/Camino de Vera s/n, 46022-Valencia, Spain.*

† Electronic Supplementary Information (ESI) available: [details of any supplementary information available should be included here]. See DOI: 00.0000/00000000.

‡ Permanent address: Unidad Multidisciplinaria de Docencia e Investigación-Juriquilla, Facultad de Ciencias, Universidad Nacional Autónoma de México (UNAM), Juriquilla, Querétaro, CP 76230, Mexico.

temperature-dependent forces of geometric and energetic origin that act on the charge carriers during transport (see the scheme in Figure 1). These forces can be interpreted consistently as entropic restrictions [13,14], that is, as drastic variations of the number of configurational microstates accessible to the charge carriers.

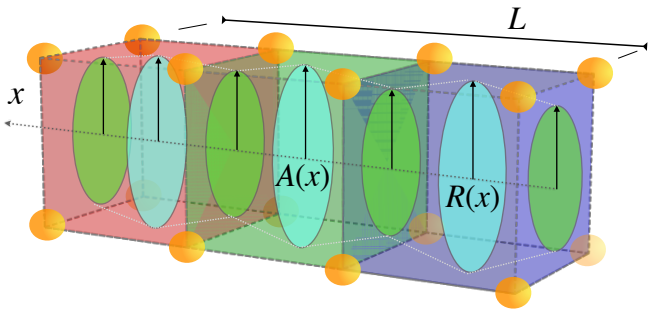

Figure 1 Schematic representation of the ionic channel (pore) with the main geometric parameters used in calculations. The presence of the atoms of the cristal matrix of length L are located at regular distances. This induces the entropic restrictions by making the transversal cross area $A(x) = \pi R^2(x)$ a function of the main transport direction x.

This discussion makes clear that the volume average has to be performed sequentially by first calculating the projection of $\mathbf{i}$ over the cross section area along the direction of main transport and, afterwards, over the longitudinal coordinate. The first average incorporates, through the boundary conditions, the constrictions (geometric and energetic) imposed on the charge carriers by the material which have been interpreted consistently as entropic restrictions [13,14], that is, as drastic reductions of the number of configurational microstates accessible to the charge carriers. These entropic constrictions enter the projected description as weights (densities of configurational states) of the longitudinal coordinate that are inversely proportional to the local width $\mathscr{A}(x)$ of the pore. Finally, the longitudinal average yields the frequency ν dependent electric current I_ν. This current satisfies a generalized Ohm's law and depends on thermodynamic parameters like the porosity ϕ, the constriction δ and the tortuosity τ factors that are the most adequate for describing the entropic restrictions mentioned and are fundamental to describe mass transport across porous media.

The model developed in the article can be complemented with the adsorption-desorption kinetics and surface diffusion processes, fact that makes it of particular interest in fuel cell design. [11,12] The mathematically simple formula we will derive provides accurate quantitative descriptions of experimental data for the ionic conductance and gives a thermodynamic interpretation of the results. Since it also establishes a rigorous connection among the microscopic geometry of the material and the macroscopic transport coefficient, it opens the possibility of design in detail the structure of the porous materials for specific solutions to required macroscopic needs of operation and rest of fuel cells, batteries and supercapacitors.

The article is divided as follows. In section 2 we introduce the model on the basis of charge and mass transport processes for systems presenting memory effects. Section 3 is then devoted to explain the effect that the irregularities of the ionic channels or pores have over the charge transport and deduce a general formula for the conductivity as function of the temperature that may involve phase changes. A model for the variation of the porosity associated with the symmetry change of the crystal structure in the superprotonic transition is introduced in section 4. Furthermore, it is used to fit different experimental data of the conductivity in terms of the temperature for systems that present the superprotonic transition. The agreement is remarkably good and the activation enthalpies obtained before and after the transition are fully consistent with previous determinations. The conclusions are presented in section 5.

2 Irreversible thermodynamics of ionic transport

Beyond the quantum mechanical details of the individual transport of ions, the physical problem associated with the impedance measurements consists in the application of a difference of electrical potential through a material. Since the material has a given different crystallographic symmetry then it should have a given porosity, even in the case of polycrystalline samples. The applied voltage induces the motion of a number of free charge carriers in the material that gives rise to an electric current. The number of free charge carriers can be characterized by the charge density per unit volume $\rho_q(\mathbf{r},t) = Qn(\mathbf{r},t)$ with Q the characteristic charge and $n(\mathbf{r},t)$ the number density of charge carriers at position $\mathbf{r}$ at time t that represents its non-homogeneous and time dependent tridimensional spatial distribution.

From an irreversible thermodynamics perspective, the electric current per unit area (having dimensions of A/m^2) obeys the relation

$$\mathbf{i}(\mathbf{r},t) = -\int_0^t \tilde{\sigma}(t-t')\frac{\partial}{\partial \mathbf{r}}\frac{\tilde{\mu}(\mathbf{r},t')}{z_i F}dt', \tag{1}$$

where $\tilde{\sigma}(t)$ is a memory function related with the ion conductivity that contemplates the non-instantaneous response of the system. [15–18] Furthermore, $\tilde{\mu}(\mathbf{r},t)$ is the *non-equilibrium electrochemical potential* given by

$$\tilde{\mu}(\mathbf{r},t) = RT\ln|\rho_q \cdot \gamma(\rho_q)| + z_i F\psi(\mathbf{r},t), \tag{2}$$

where $\gamma(\rho_q)$ is an activity coefficient that introduces all the non-idealities associated with the direct interaction among charge carriers. The electrovalency of the charge carriers is denoted by z_i, the Faraday constant by F and the electrical potential by $\psi(\mathbf{r},t)$. This potential may be originated by an external agent ψ_{ext} and a charge distribution ϕ_{int} over the walls of the pores: $\psi(\mathbf{r},t) = \phi_{int}(\mathbf{r}) + \psi_{ext}(\mathbf{r},t)$.

The Fourier transform of eqn (1) yields

$$\mathbf{i}_\nu = -\frac{\sigma_\nu^*}{z_i F}\frac{\partial}{\partial \mathbf{r}}\tilde{\mu}_\nu, \tag{3}$$

where $\mathbf{i}_\nu \equiv \mathbf{i}(\mathbf{r},\nu)$ and $\tilde{\mu}_\nu \equiv \tilde{\mu}(\mathbf{r},\nu)$. The complex conductivity $\sigma_\nu^* \equiv \sigma^*(\nu;T)$ may depend on the temperature, and on the frequency ν if an alternate electric field is applied to the system through its boundaries at the ends of the material.

The theoretical determination of this conductivity is a difficult task. However, general results from the theory of absolute rate

processes [19,20] show that its temperature dependence is, in general, proportional to an Arrhenius-like law that can be written in the form

$$\sigma_\nu^* \propto \sigma_{\nu,0}^* T\, e^{-\Delta G^\ddagger / k_B T}. \tag{4}$$

Here, σ_ν^* is now only a function of the frequency,[8] $\Delta G^\ddagger$ is the activation Gibbs free energy of the microscopic conduction process in the material and we have written explicitly the proportionality of this elementary rate with the temperature T for convenience. The eqn (4) is consistent with the temperature dependence of $G_\nu(T)$ when no phase transformations are present. The frequency dependence is usually proposed in an *ad hoc* form or by following semi-empirical models. However, a systematic approach can be found in the literature.[16] A final pertinent comment is that adding noise to eqn (1) makes possible a stochastic description of single particle processes at different levels, like in Refs. [21,22].

3 Ionic macrotransport in irregular domains

At a given temperature, the conductance $G_\nu(T)$ is the proportionality constant between the ion current I_ν and the voltage V_ν applied on the system in agreement with the generalized Ohm's law:

$$I_\nu = G_\nu V_\nu, \tag{5}$$

which means that the fundamental relation eqn (3) for the current density must be *averaged* over the volume of the system in order to be consistent with eqn (5). In most theoretical analysis it is commonly obviated that this average procedure has to consider the particular geometry of the structures or pores along the which the ions move. Thus, the boundary conditions introduced by these irregular domains on the transport may not be trivially introduced in the resulting transport relation and may have important consequences on the average transport properties. In this section we will show how this volume average has to be done and the important implications it has on the ionic macrotransport. The theory will be constructed in analogy with that for mass transport across pores.[11]

The first step is to calculate the projected electric current i_ν, defined by the well known relation: $i_\nu = \int \mathbf{i}_\nu \cdot d\mathbf{A}$, with $d\mathbf{A}$ the element of cross section area along the direction of main transport, x. Hence, in the simplest case, the irregularities of the boundaries can be described by a position dependent radius $R(x)$ that enters in the projection of eqn (3) through the integral limits, as follows

$$i_\nu = -\frac{\sigma_\nu^*}{z_i F}\int_0^{2\pi}\int_0^{R(x)} \frac{\partial \tilde{\mu}_\nu}{\partial x} r dr d\theta, \tag{6}$$

where we have assumed that σ_ν^* is independent of the transverse coordinates. Using the Leibniz rule, eqn (6) yields

$$i_\nu = -2\pi \frac{\sigma_\nu^*}{z_i F}\left[\frac{\partial}{\partial x}\int_0^{R(x)} \tilde{\mu}_\nu r dr - R(x)\,\tilde{\mu}_\nu(x,R)\frac{\partial R}{\partial x}\right]. \tag{7}$$

For large enough pores [$L >> R(x)$] we can assume homogeneity along the radial direction:[11] $\tilde{\mu}_\nu(x,r,t) \simeq \tilde{\mu}_\nu(x,t)$ and therefore the integral in the first term of eqn (7) gives $\tilde{\mu}_\nu R^2(x)/2$.

Algebraic manipulations make possible to rewrite eqn (7) in the compact form

$$\frac{i_\nu}{\sigma_\nu^* \mathscr{A}(x)} = -\frac{\partial}{\partial x}\left(\frac{\tilde{\mu}_\nu}{z_i F}\right), \tag{8}$$

where $\mathscr{A}(x) \equiv \pi R^2(x)$ is the transversal area of the pore at position x.

The volume average may now be completed by integrating eqn (8) over the x direction from 0 to L, with L the longitudinal size of the system. Noticing that the electric current I_ν should be independent of x for any size L of the system, it is usually assumed that the local variations of the projected current are negligible and then $i_\nu \simeq I_\nu$. Therefore, the integration of eqn (8) yields the macrotransport flux-force relation

$$I_\nu \int_0^L \frac{dx}{\sigma_\nu \mathscr{A}(x)} = -\frac{\Delta\tilde{\mu}_\nu}{z_i F}, \tag{9}$$

which establishes that the electric current is proportional to the macroscopic difference of the electrochemical potential: $\Delta\tilde{\mu}_\nu = \tilde{\mu}_\nu(L) - \tilde{\mu}_\nu(0)$. For large enough voltages, V_ν, the contribution of the diffusion term can be neglected and hence, we recover the well known relation: $\Delta\tilde{\mu}_\nu/z_i F = \Delta\psi = -V_\nu$.

Introducing now the maximum cross area $\mathscr{A}_{max}$ of a system's cell,[12] the integral in eqn (9) can be written as the inverse average conductivity $\hat{\sigma}_\nu$ of the system

$$\frac{1}{\hat{\sigma}_\nu} \equiv \frac{1}{L}\int_0^L \frac{dx}{\sigma_\nu\, \Omega(x)}, \tag{10}$$

where we have defined: $\Omega(x;T) = \mathscr{A}(x;T)/\mathscr{A}_{max}$. Using these relations, eqn (9) can be written as a generalized Ohm's law where one identifies the conductance $G_\nu(T)$ as

$$G_\nu(T) = \hat{\sigma}_\nu(T)\frac{\mathscr{A}_{max}}{L}. \tag{11}$$

The eqn (10) is very important since it can be used to introduce a temperature dependence of the conductance that goes beyond the Arrhenius law and makes the macrotransport description able to describe ion conductivity in a wider range of temperatures in a more direct and consistent way than it is actually done.

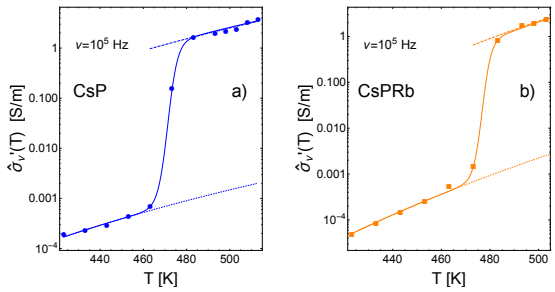

Figure 2 The solid lines are the fits using eqns (17) and (19) of the real part of the conductivity $\hat{\sigma}_\nu(T)$ as a function of temperature (including a superprotonic transition) for the experimental data (symbols) of doped cesium phosphates studied in Ref.[8]. The dotted and dashed lines represent the Arrhenius behaviors, eqn (4), far from the transition region.

The temperature dependence enters into the description through the dimensionless width factor of the pores, $\Omega(x)$, since it

Table 1 Parameters used for fitting the real part of the conductivity $\hat{\sigma}_\nu(T)$ as a function of the temperature, for $\nu = 10^5$ Hz. Fits are shown in Figure 1 of the main text.

	$\sigma_{\nu,0}$ [S/m]	$\Delta H^\ddagger$[eV]	$\Delta H^\ddagger_{sp}$[eV]	β[K]	T_c [K]	α [K^{-1}]	ϕ_c	ε
CsP	2.0 x 10^{-4}	0.468	0.468	1.95	472.2	2.0 x 10^{-2}	0.45	0.0
CsPRb	5.0 x 10^{-5}	0.850	0.850	1.75	476.7	1.4 x 10^{-2}	0.54	0.0

can be related with the local entropy restrictions that the porous matrix $[\delta s_m(x)]$ of the material imposes over the charge carriers. These entropy restrictions are linked with the crystallographic symmetry that depends on temperature. This dependence has been postulated in the form [13,14,23]

$$\delta s_m(x;T) = s_{m,max} - s_m(x;T) = -k_B \ln|\Omega(x;T)| > 0. \tag{12}$$

Using this relation and assuming that σ^*_ν is independent of the position, eqn (10) yields

$$\hat{\sigma}_\nu = \frac{\sigma^*_\nu}{(1/L)\int_0^L e^{\delta s_m/k_B} dx} \simeq \sigma^*_\nu e^{-\Delta S_m/k_B}, \tag{13}$$

where the symbol $\Delta S_m(T)$ should be interpreted as the macroscopic change of the entropy constrictions within the system as a function of the temperature. This implies that it can be related with the change of conductivity when structural or phase transitions between crystallographic symmetries occurs.

In writing eqn (13), we have assumed that the first order term of a cumulant expansion is the leading term, and therefore $\langle e^{\delta s_m/k_B}\rangle \simeq e^{\langle \delta s_m\rangle}/k_B = e^{\Delta S_m/k_B}$, where the brackets indicate the spatial average.

Using now eqn (4) and eqn (13), we obtain the final formula for the electric conductivity

$$\hat{\sigma}_\nu \propto \sigma^*_{\nu,0}\, T\, e^{-\Delta G^\ddagger/k_B T} e^{-\Delta S_m/k_B}. \tag{14}$$

The quantity $\Delta S_m(T)$ is a thermodynamic excess entropy associated with the macroscopic structural changes of the material that give rise to entropic restrictions during the motion of the charge carriers. In contrast, the free energy $\Delta G^\ddagger$ corresponds to the microscopic elemental rate process that can be determined, in principle, by using transition state theories. [19,20]

4 Entropy constrictions in the superprotonic transition of solid electrolytes

It is well known that the thermal behavior of the conductivity of some solid acids such as RbH2PO4, CsHSO4 and CsH2PO4 have a superprotonic phase transition (SPT) in which a drastic increase in conductivity of several orders of magnitude is observed. [4–8] That is, the experiments determine the conductivity of the solid electrolytes in terms of temperature for ranges in which the superprotonic transition takes place. Recently, for instance, broadband dielectric and DSC thermal analysis were used to correlate the superprotonic transition of different solid compounds of cesium phosphate and other solid electrolytes with the structural transition between monoclinic ($T < T_c$ with T_c the transition temperature) and cubic symmetries ($T > T_c$). [8,24]

In this section, we will use eqn (14) in order to cope with experimental measurements of the electric conductivity as a function of the temperature and show that the superprotonic transition can be adequately explained in terms of the thermodynamic excess entropy associated with the macroscopic structural changes among different crystallographic symmetries of the material due to a phase or structural transition. In doing this, we first note that the structure factor of a system, expressed in terms of its phonon density of states may be indicative of the characteristic length of the corresponding crystallographic phase and, therefore, from a thermodynamic perspective, it may be associated with its density or, more usefully, with the porosity ϕ of the material.

In the case of our interest, it is convenient to consider simulation results on tetracyanoethylene crystal [25] that report the structure factor or, equivalently, the phonon density of states for monoclinic and cubic phases. It was shown that the structure factor of the monoclinic phase has a peak at frequencies near 8THz, whereas for the cubic phase the peak appears at frequencies near 3THz. [25] Since the wave number k and the frequency ν of the phonons can be related through the dispersion relation $C_{sound} = \nu/k$, one then infers that the characteristic length of the monoclinic phase ($\lambda_{mn} \sim 1/k_{mn}$) is smaller than the characteristic length of the cubic phase $\lambda_c >> \lambda_{mn}$, where the subindexes correspond to the cubic (c) and monoclinic (mn) phases, respectively. From the above mentioned thermodynamic perspective, this difference implies that the cubic phase should be more porous than the monoclinic phase, that is, $\phi_c > \phi_{mn}$. These results are consistent with our experimental measurements on the conductivity [8] in which the cubic phase shows a three orders of magnitude larger conductivity than the monoclinic phase, see Figure 1. Since the porosity is proportional to the average width of the pores $\phi \propto \langle \mathscr{A} \rangle$, [11] and in analogy with eqn (12), in first approximation we may introduce the relation

$$\Delta S_m(T) = -\alpha\, k_B T_c \ln\left|\frac{\phi(T)}{\phi_{mn}}\right|. \tag{15}$$

The eqn (15) can be calculated by using the Clapeyron equation for the solid-solid phase transition after considering that the volume can be expressed as a function of the porosity ϕ, using the definition of the thermal expansion coefficient α and the experimental evidence on the dependence of the pressure on the porosity, $P(\phi) \sim \phi^{-1}$, see Refs. [26,27] and the ESI for details.

An *ad hoc* model accounting for the behavior of the porosity in terms of the temperature corresponding to the monoclinic to cubic transition around the temperature T_c can be formulated using the sigmoidal function

$$\phi(T) = \phi_{mn} + \frac{(\phi_c - \phi_{mn})}{1 + e^{-(T-T_c)/\beta}} \left(\frac{T}{T_c}\right)^\varepsilon, \tag{16}$$

Table 2 Parameters used for fitting the real part of the conductivity $\hat{\sigma}_v(T)$ as a function of the temperature of Figure 2 of the main text.

	$\sigma_{v,0}[S/m]$	$\Delta H^{\ddagger}$ [eV]	$\Delta H^{\ddagger}_{sp}$ [eV]	β	$T_c[K]$	α	ϕ_c	ε
$Cs_2(HSO_4)(H_2PO_4)$	6.6×10^{-4}	0.132	0.110	1.67	356.0	1.6×10^{-2}	0.48	−0.2
CsH_2PO_4	3.8×10^{-1}	0.105	0.105	1.14	498.0	1.5×10^{-2}	0.30	0.0
$CsHSO_4$	5.2×10^{-2}	0.202	0.137	0.50	404.0	1.8×10^{-2}	0.31	−0.7
RbH_2PO_4	1.5×10^{-2}	0.386	0.217	3.57	549.0	4.5×10^{-3}	0.42	−2.8

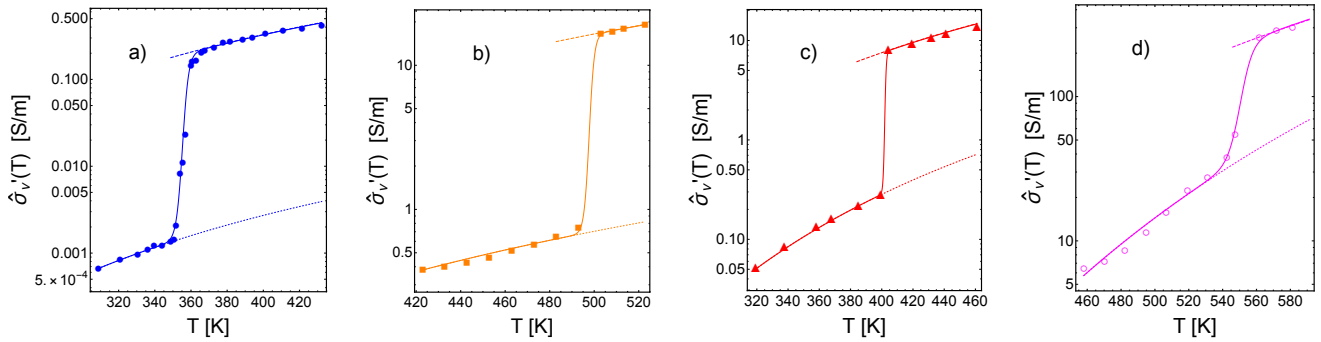

Figure 3 The solid lines are the fits using eqns (17) and (19) of the real part of the conductivity $\hat{\sigma}_v(T)$ as a function of temperature (including a superprotonic transition) for the experimental data (symbols) of different compounds reported in the literature. a) Data of $Cs_2(HSO_4)(H_2PO_4)$ salts taken from Ref. 4. b) Data of CsH_2PO_4 salts taken from Ref. 6.c) Data of $CsHSO_4$ salts taken from Ref. 5.d) Data of RbH_2PO_4 salts taken from Ref. 8.The dotted and dashed lines are the partial Arrhenius behaviors taking place far from the transition region.

where β and ε are fitting parameters. The parameter β is a measure of the transition width, that is, how narrow is the transition to the superprotonic phase in Kelvins, and ε is an exponent which determines the change of slope of the conductivity after the transition, that is, it is related to an enthalpy change of the new phase with respect to the original one. Using eqn (16) into eqn (15) we obtain

$$\Delta S_m(T) = -\alpha\, k_B T_c \ln\left|\phi_{mn} + \frac{(\phi_c - \phi_{mn})}{1+e^{-(T-T_c)/\beta}}\left(\frac{T}{T_c}\right)^{\varepsilon}\right|, \qquad (17)$$

which is the expression for the excess entropy giving rise to the entropic restrictions.

4.1 Comparison with experiments

It is necessary here to introduce some pertinent considerations related with the usual determination of the experimental activation energy E_a by using the standard Arrhenius formula of the form $\sigma = Ce^{-E_a/kT}$, in which C is a constant.

The relation between the Gibbs free energy of activation and E_a can be established by introducing the thermodynamic relation $\Delta G^{\ddagger} = \Delta H^{\ddagger} - T\Delta S^{\ddagger}$ where $\Delta H^{\ddagger}$ and $\Delta S^{\ddagger}$ are the activation enthalpy and entropy of the microscopic transport process. The resulting expression for the conductivity takes the form

$$\hat{\sigma}_v \propto \sigma^{*}_{v,0}\, T\, e^{\Delta S^{\ddagger}/k_B} e^{-\Delta H^{\ddagger}/k_B T} e^{-\Delta S_m/k_B}, \qquad (18)$$

where $\Delta S^{\ddagger}$ is a constant quantity within the temperature range in which the conductivity behaves following an Arrhenius-like behavior. The entropic $\Delta S_m(T)$ correction absorbs the temperature dependence in the whole temperature range, that may present superprotonic transitions.

For data fit it is convenient to take the value of the conductivity at the initial temperature T_0, $\hat{\sigma}_v(T_0)$, as a reference value. Using these results and the eqn (17) we obtain the following formula for the electric conductivity

$$\frac{\hat{\sigma}_v}{\hat{\sigma}_v(T_0)} = \frac{T}{T_0} e^{-\frac{1}{k_B}\left(\frac{1}{T}-\frac{1}{T_0}\right)\Delta H^{\ddagger}} e^{-[\Delta S_m(T)-\Delta S_m(T_0)]/k_B}, \qquad (19)$$

where $\Delta S_m(T)$ is given by eqn (18).

The symbols in Figure 1 show the conductivity as a function of the temperature for pure polycrystalline acidic salts of cesium di-hydrogen phosphate CsH_2PO_4 (CsP), and mixtures of 80:20 w/w of CsH_2PO_4 with RbH_2PO_4 (CsPRb), $CsHMoO_4$ (CsPMo), $CsHWO_4$ (CsPW), as indicated in each case. The data were collected from dielectric spectroscopy using an alternate electric field with frequency $\nu = 10^5$ Hz. For the details of the sample synthesis and of the experimental protocol to determine the conductivity see Ref.[8] For a given collecting frequency, the conductivity is solely a function of temperature. It is clear from the results of Figure 1, that the range of temperatures studied involves a superprotonic transition associated with a solid phase transition between monoclinic to cubic symmetries about $T \sim 475\,K$ in all the mixtures considered here. The values of the parameters used are given in Table 1.

The enthalpy difference $\Delta H^{\ddagger}$ was used to fit the slope of the conductivity in the temperature range before the transition, that is, $T \in (423, 460)$ K. The whole temperature range behavior (solid lines) is reproduced by the eqns 14 and 19. For low ($T < T_c$) and high ($T > T_c$) temperatures an Arrhenius behavior is obeyed, see the dotted and dashed lines, respectively. The enthalpy difference $\Delta H^{\ddagger}_{sp}$ after the superprotonic transition can be determined by the

formula

$$\Delta H^{\ddagger}_{sp} \simeq \Delta H^{\ddagger} + \varepsilon\, \alpha\, T_c^2\, \delta_\phi \frac{y_{sp}^{\varepsilon+1}}{1+\delta_\phi y_{sp}^{\varepsilon}}, \tag{20}$$

where $\delta_\phi \equiv (\phi_c - \phi_{mn})/\phi_{mn}$ and $y \equiv \langle T_{sp}\rangle / T_c$. The eqn (20) was obtained by equating the slopes of the general formula eqn (19) and of an Arrhenius law with $\Delta H^{\ddagger}_{sp}$ [see eqn (4)] for any temperature T larger than T_c. Therefore, an optimal form to determine the value of the enthalpy difference $\Delta H^{\ddagger}_{sp}$ after the superprotonic transition is by performing the arithmetic average of the experimental temperatures after the transition, $\langle T_{sp}\rangle$. The eqn (20) shows that the parameter ε is proportional to the difference of the activated enthalpies before and after the superprotonic transition, as mentioned before. The values of $\Delta H^{\ddagger}_{sp}$ are also reported in the Table 1.

For all salts it was assumed that the porosity of the monoclinic phase is about $\phi_{mn} = 0.2$. These values could vary from sample to sample and are rough estimates due to the lack of experimental information. Nonetheless, changing them does not affect the shape of the solution but the amplitude of the conductivity leap due to the phase transition. The variation of the porosity in the numerical fits may be readjusted *via* the thermal expansion coefficient α. Hence, an accurate determination of the porosity is reflected in an more accurate value of α or viceversa. The data in Figure 1 were fitted using $\varepsilon = 0$, which means that the activation enthalpy for the new structure is similar to that of the original one. The Figure 2 shows different comparisons between our theory and conductivity measurements for several samples taken from the literature, see the caption for details. All these salts display a structural phase transition from monoclinic phase to cubic phase in $Cs_2(HSO_4)(H_2PO_4)$ and CsH_2PO_4 samples, to a tetragonal phase in $CsHSO_4$ and to non-indentified phase in the RbH_2PO_4 sample. The agreement is excellent and the values of the activation enthalpies consistent with previous determinations. Three systems have a negative value of ε, indicating a decrease of the activation enthalpy after the superprotonic transition. All the parameters used for fitting the conductivities in Figures 1 and 2 are included, respectively, in Tables 1 and 2.

4.2 Generalization of the conductivity formula to more complex topologies

A more general expression of eqn (15) follows after noticing that ΔS_m not only depends on ϕ. In fact, ΔS_m also depends on the internal topology of the conducting channels or pores in such a way that it can be predicted on geometrical basis. From the macroscopic point of view, the internal topology is characterized by means of the constriction (δ) and the tortuosity (τ) factors.[12,28] The relation is

$$\Delta S_m = -\alpha\, k_B T \ln\left|\frac{\phi\,\delta}{\tau}\right|. \tag{21}$$

For systems having a linear dependence with temperature of the thermal expansion coefficient[29] the substitution of the eqn (21) into eqn (13) yields the following simple relation for the conductivity: $\hat{\sigma}_v \simeq \sigma_v^* \frac{\phi\delta}{\tau}$. This expression is consistent with an empirical relation for the effective diffusivity D_c of a membrane: $D_c \simeq D_0 \frac{\phi\delta}{\tau}$ obtained by performing mass diffusion experiments.[12,30]

5 Conclusions

We have formulated a macrotransport theory for calculating a very general and powerful expression for the electric conductivity as a function of the temperature. The expression generalizes the well known Arrhenius behavior and shows that the superprotonic transition occurs due to a change of the entropic restrictions associated with the structure of the material, appropriately characterized in terms of porosity, constriction and tortuosity factors. Remarkably good fits were obtained for the conductivity of different solid electrolytes that present an structural or phase transition in the temperature range considered and therefore the corresponding thermodynamic properties are obtained, like the activation enthalpy and entropy, that is, the Gibbs free energy.

Our theory improves the understanding and prediction of the performance of solid state electrolytes of fuel cells as well as batteries, supercapacitors, catalytic materials, controlled delivery materials and ion-conductors. Furthermore, it opens a new branch in the study of stable inorganic backbones whose conductivity properties may vary depending on the sought applications of the materials in the technological systems already listed.

Conflicts of interest

There are no conflicts to declare.

Acknowledgements

ISH, SIH, CGA and ALD acknowledge financial support by UNAM-DGAPA under grants IN 116617, IN117419 and IA104319. V. Compañ is grateful to Ministerio de Economía y Competitividad (MINECO), project reference: ENE/2015-69203-R. SIH is grateful to project LANCAD-UNAM-DGTIC-276. ALD acknowledge DGAPA-UNAM CJIC/CTIC/4692/2019. ISH acknowledges Prof. Víctor Castaño for his hospitality during a sabbatical leave in which this work was finished.

Notes and references

1 A. I. Baranov, V. P. Khiznichenko and L. A. Shuvalov, *Ferroelectrics*, 1989, **100**, 135–141.

2 A. I. Baranov, V. P. Khiznichenko, V. A. Sandler and L. A. Shuvalov, *Ferroelectrics*, 1988, **81**, 183–186.

3 A. Baranov, B. Merinov, A. Tregubchenko, V. Khiznichenko, L. Shuvalov and N. Schagina, *Solid State Ionics*, 1989, **36**, 279 – 282.

4 C. R. Chisholm and S. M. Haile, *Solid State Ionics*, 2000, **136-137**, 229 – 241.

5 I. N. Bagryantseva and V. G. Ponomareva, *Phys. Solid State*, 2016, **58**, 1651–1658.

6 J. Otomo, T. Ishigooka, T. Kitano, H. Takahashi and H. Nagamoto, *Electrochimica Acta*, 2008, **53**, 8186 – 8195.

7 Z. Li, *Electrochimica Acta*, 2010, **55**, 7298 – 7304.

8 A. Andrio, S. I. Hernández, C. García-Alcántara, L. F. del Castillo, V. Compan and I. Santamaría-Holek, *Phys. Chem. Chem. Phys.*, 2019; DOI: 10.1039/C8CP07472K.

9 J. Montes, F. Cuevas and J. Cintas, *Appl. Phys. Mater. Sci. Process.*, 2008, **92**, 375–380.

10 M. Liu, L. Chen, S. Y. Chong, M. A. Little, T. Hasell, I. M. Aldous, C. M. Brown, M. W. Smith, C. A. Morrison, L. J. Hardwick, A. I. Cooper and S. Lewis, *Nat. Comm.*, 2016, **7**, 12750.

11 A. Ledesma-Durán, S. I. Hernández and I. Santamaría-Holek, *J. Phys. Chem. C*, 2017, **121**, 14544–14556.

12 A. Ledesma-Durán, S. I. Hernández Hernández and I. Santamaría-Holek, *J. Phys. Chem. C*, 2017, **121**, 14557–14565.

13 R. Zwanzig, *J. Phys. Chem.*, 1992, **96**, 3926–3930.

14 D. Reguera and J. M. Rubí, *Phys. Rev. E*, 2001, **64**, 061106.

15 I. Goychuk, *Phys. Chem. Chem. Phys.*, 2018, **20**, 24140.

16 H. Híjar, J. G. Méndez-Bermúdez and I. Santamaría-Holek, *J. Chem. Phys.*, 2010, **132**, 084502.

17 R. Hernández and F. L. Somer, *J. Phys. Chem. B*, 1999, **103**, 1064–1069.

18 R. Zwanzig, *J. Chem. Phys.*, 1970, **52**, 3625–3628.

19 A. García-Bernabe, V. Compan, M. I. Burguete, E. García-Verdugo, N. Karbass, S. V. Luis and E. Riande, *J. Phys. Chem. C*, 2010, **114**, 7030–7037.

20 H. Eyring, *J. Chem. Phys.*, 1935, **3**, 107–115.

21 I. Goychuk, *Phys. Chem. Chem. Phys.*, 2017, **19**, 3056.

22 N. Palma-Aramburu and I. Santamaría-Holek, *Phys. Rev. E*, 2017, **96**, 022103.

23 I. Santamaría-Holek, Z. Grzywna and J. Rubi, *Eur. Phys. J. Spec. Top.*, 2013, **222**, 129–141.

24 J. Otomo, N. Minagawa, C. ju Wen, K. Eguchi and H. Takahashi, *Solid State Ionics*, 2003, **156**, 357 – 369.

25 B. Schatschneider, J.-J. Liang, S. Jezowski and A. Tkatchenko, *Cryst. Eng. Comm.*, 2012, **14**, 4656–4663.

26 M. M. Carroll and K. T. Kim, *Powder Metall.*, 1984, **27**, 153–159.

27 J. Walder and A. Nur, *J. Geophys. Res. Solid. Earth.*, 1984, **89**, 11539–11548.

28 M. Agarwal and C. Chakravarty, *Phys. Rev. E*, 2009, **79**, 030202.

29 K. Joseph, M. C. Stennett, N. C. Hyatt, R. Asuvathraman, C. L. Dube, A. S. Gandy, K. G. Kutty, K. Jolley, P. V. Rao and R. Smith, *J. Nucl. Mater.*, 2017, **494**, 342 – 353.

30 L. F. del Castillo, S. I. Hernández and V. Compan, *Membranes (Materials, Simulations and Applications), Chapter 9*, Springer International Publishing, Switzerland, 2017.